Biophysical Chemistry 146 (2010) 42–53

Contents lists available at ScienceDirect

Biophysical Chemistry

journal homepage: http://www.elsevier.com/locate/biophyschem

Nanogravimetric and voltammetric DNA-hybridization biosensors for studies of DNA damage by common toxicants and pollutants

Anna M. Nowicka [a,b], Agata Kowalczyk [b], Zbigniew Stojek [b], Maria Hepel [a,*]

[a] Department of Chemistry, State University of New York at Potsdam, Potsdam, New York 13676, USA
[b] Department of Chemistry, University of Warsaw, PL-02-093 Warsaw, Poland

ARTICLE INFO

Article history:
Received 3 September 2009
Received in revised form 5 October 2009
Accepted 5 October 2009
Available online 12 October 2009

Keywords:
DNA-hybridization sensor
DNA damage
Pesticide
Cr(VI)
Herbicide
Toxicants

ABSTRACT

Electrochemical and nanogravimetric DNA-hybridization biosensors have been developed for sensing single mismatches in the probe-target ssDNA sequences. The voltammetric transduction was achieved by coupling ferrocene moiety to streptavidin linked to biotinylated tDNA. The mass-related frequency transduction was implemented by immobilizing the sensory pDNA on a gold-coated quartz crystal piezoresonators oscillating in the 10 MHz band. The high sensitivity of these sensors enabled us to study DNA damage caused by representative toxicants and environmental pollutants, including Cr(VI) species, common pesticides and herbicides. We have found that the sensor responds rapidly to any damage caused by Cr(VI) species, with more severe DNA damage observed for $Cr_2O_7^{2-}$ and for CrO_4^{2-} in the presence of H_2O_2 as compared to CrO_4^{2-} alone. All herbicides and pesticides examined caused DNA damage or structural alterations leading to the double-helix unwinding. Among these compounds, paraoxon-ethyl and atrazine caused the fastest and most severe damage to DNA. The physicochemical mechanism of damaging interactions between toxicants and DNA has been proposed. The methodology of testing voltammetric and nanogravimetric DNA-hybridization biosensors developed in this work can be employed as a simple protocol to obtain rapid comparative data concerning DNA damage caused by herbicide, pesticides and other toxic pollutants. The DNA-hybridization biosensor can, therefore, be utilized as a rapid screening device for classifying environmental pollutants and to evaluate DNA damage induced by these compounds.

Published by Elsevier B.V.

1. Introduction

The increasing environmental pollution, caused by expanding industrialization and application of new intensive agricultural technologies, necessitates urgent development of pollution monitoring [1,2] and novel methods for fast screening of harmful compounds. Of a particular importance are bioactive pollutants causing DNA damage [3–7], carcinogenesis [8–10], and a number of different diseases. In this work, we report on the design and testing of a novel biosensor based on unique sensitivity of DNA hybridization process to DNA damage and structural alterations caused by pollutants, such as Cr(VI), herbicides and pesticides.

Herbicides and pesticides are very serious environmental pollutants [5,11]. They show a high acute toxicity and a wide range of biological activities [6,12–15]. It is believed that active herbicides/pesticides in combination with adjuvants used in agricultural preparations are the main source of genotoxicity [16]. The Codex Alimentarius Commission of the Food and Agriculture Organization (FAO) and the World Health Organization (WHO) have established maximum residue limits for pesticides in food [12]. Standard procedures, based on liquid chromatography and gas chromatography, are reliable techniques for routine laboratory detections of pesticides. However, there is also a need for innovative methods for rapid, inexpensive, and field-deployable testing. Recently, we have developed highly sensitive piezoimmunosensors for the detection of herbicides, atrazine [17] and 2,4-D [18]. Disposable immuno-electrochemical sensors for herbicides have been developed by Helali et al. [19].

Various types of biosensors have been developed in the field of environmental monitoring [20–22]. The DNA biosensors have recently gained some importance in such applications. For instance, the DNA biosensors have been employed in diagnostics, gene analysis, fast detection of biological warfare agents, detection of genetically modified food, and forensic applications [23–30]. Oliveira-Brett and coworkers [31] applied DNA sensors for elucidation of anticancer drug interactions with DNA. The key part of these biosensors is a molecular probe that is built from oligonucleotides of well defined sequence. That sequence must be complementary to the oligonucleotide sequence to be detected. The hybridization process is specific and only the complementary strands can hybridize. Many different transduction techniques have been applied to convert the information on the progress of DNA hybridization to an analytical signal, such as the electrochemical [32–35], impedimetric [36], or spectroscopic tagging of nucleotides under test [37,38].

* Corresponding author. Fax: +1 315 267 3170.
E-mail address: hepelmr@potsdam.edu (M. Hepel).

0301-4622/$ – see front matter. Published by Elsevier B.V.
doi:10.1016/j.bpc.2009.10.003

Two fundamental issues that need to be addressed in the development of DNA hybridization sensors are related to the specificity and selectivity of the devices [39]. The DNA biosensors based on the avidin–biotin affinity fit very well these issues [40–43]. Biotin is a small molecule that binds with a very high affinity to the avidin- or streptavidin binding sites ($K_a = 10^{15} M^{-1}$) [44,45]. The utility of the streptavidin–biotin interactions follows from the dihedral D_2 molecular symmetry of the streptavidin which makes it possible to bind two pairs of biotin on opposite faces of the protein [46] and in consequence this opens the possibility to construct multilayer architectures [38,47,48]. Streptavidin is extremely resistant to thermal denaturation and chaotropes [49], and many biotinylated molecules are commercially available. The applications of these electroinactive proteins in DNA hybridization biosensors with electrochemical detection require introducing a charge mediator which is either a freely diffusing electron-transfer shuttle or an attached redox relay. Ferrocene derivatives are very often used as charge mediators because of their desirable properties, including electrochemical reversibility, high Fc^0/Fc^+ electron self-exchange rates of ~10^7 $mol^{-1} dm^3 s^{-1}$ [50], and its adjustable formal potential over a considerable range which is achieved by introducing appropriate substituents into the cyclopentadienyl ring. The electron relaying via ferrocene bound through a flexible chain to the protein surface has been extensively studied in recent years [51–55].

The methods used for the detection of DNA hybridization process include electrochemical [35,56–63], optical [37,64–66], impedimetric [36], surface plasmon resonance [67] and microgravimetric techniques [68–71]. The electrochemical quartz crystal nanobalance (EQCN) has been employed in ultra-sensitive biosensor applications [30,38,72–74] including aptamers [75] and immunosensors [17,18,76]. The crystal resonance frequency decreases with increasing mass of the sensory film attached to the gold piezoelectrode [77]. With EQCN, subnanogram levels of mass change can be detected. Higher sensitivity is achieved by using QCN crystals of higher frequencies [78]. Further enhancement of the detection can be obtained, if necessary, by amplification of the nucleic acids by polymerase chain reaction (PCR) [79].

In this report, we propose a new diagnostic method of testing DNA damage by pollutants based on the DNA hybridization sensing with electrochemical and nanogravimetric transduction. A specific DNA

Herbicides:

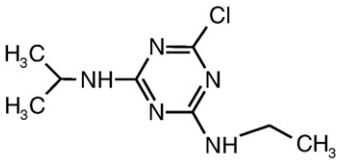

atrazine

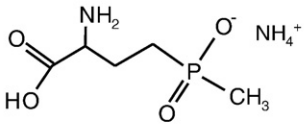

glufosinate ammonium (GA)

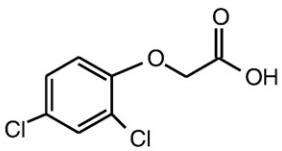

2,4-dichydrophenoxyacetc acid (2,4-D)

Pesticides:

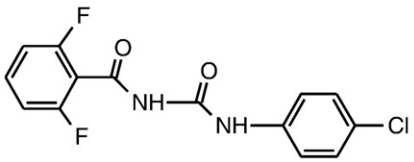

diflubenzuron (DFB)

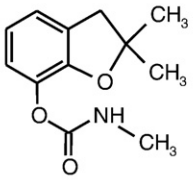

carbofuran (CF)

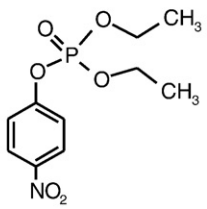

Paraoxon-ethyl (PE)

Scheme 1. Structural formula of tested herbicides and pesticides.

hybridization biosensor was designed utilizing the affinity of biotinylated ssDNA to streptavidin. The hybridization process of biotinylated single-stranded target DNA (bt-DNA) and the immobilized single-stranded probe-DNA (p-DNA) chains was carried out in the sensory film formed on a gold-coated quartz crystal piezoresonator surface. The electrochemical transducer (ferrocene labeled streptavidin) was attached at the outermost layer. Tests were performed to demonstrate a single base ssDNA mismatch sensitivity of the biosensor and subsequently to analyze the DNA damage due to Cr(VI) species, and selected herbicides and pesticides.

2. Materials and methods

2.1. Chemicals

All oligonucleotides used were purchased from MWG-Operon (Eurofins, US). The following sequences were used:

- Biotinylated probe DNA (bp-DNA):
  (5′⇨3′) biotin-ATTCGACAGGGATAGTTCGA
- Complementary modified target DNA (bt-DNA):
  (5′⇨3′) biotin-TCGAACTATCCCTGTCGAAT (designed from the ssrA gene of *Listeria monocytogenes*, a common food pathogen)
- Complementary non-modified target DNA (t-DNA):
  (5′⇨3′) TCGAACTATCCCTGTCGAAT
- C–A mismatch complementary modified target DNA (bt-DNA*):
  (5′⇨3′) biotin-TCGAACTATCACTGTCGAAT
- C–A and G–A double-mismatch complementary modified target DNA (bt-DNA**):
  (5′⇨3′) biotin-TCGAACTATCACTATCGAAT
- Non-complementary DNA strand:
  (5′⇨3′) biotin-ATTCGACAGGGATAGTTCGA.

11-mercapto-1-undecanol (MUD), 1,6-hexanedithiol (HDT), and streptavidin (SA) from *Streptomyces avidinii* were purchased from Sigma-Aldrich. Biotinylated tri(ethylene glycol) undecane thiol (bMUD) was purchased from NanoScience Instruments. All applied pesticides and herbicides were purchased from Sigma-Aldrich, and their structural formulas are presented in Scheme 1.

Two buffers were used in this work: (i) the immobilization buffer, applied in the immobilization of biotinylated probe bp-DNA, was composed of 0.15 mM NaCl, 2 mM KCl and 0.02 M phosphate buffer with pH 7.4; (ii) the hybridization buffer, composed of 1 M NaCl, 2 mM KCl and 0.02 M phosphate buffer with pH 7.4. The pH was adjusted with either NaOH or HCl solution.

2.2. Synthesis of ferrocene-labeled streptavidin (Fc-SA)

The redox labeled protein was synthesized according to the following procedures reported in the literature [48,52]. The steps in the synthesis are presented in Scheme 2.

2.2.1. N-(ferrocenylmethyl)-6-aminocaproic acid (Fc6ac).

Synthesis of this compound was performed according to Padeste et al. [52] and optimized to yield a well-defined product. To a solution of 2.75 g (12.8 mmol) ferrocene-aldehyde (Fisher) in 40 mL DMF (Sigma Aldrich) 1.5 g (11.4 mmol) 6-aminocaproic acid (Sigma Aldrich) in 10 mL 2 M NaOH were added and refluxed at 80 °C for 2 h. After cooling to room temperature, 1.25 g (33 mmol) $NaBH_4$ in 10 mL H_2O was added in small quantities. After 1 h of reaction time, acetic acid (10% in H_2O) was slowly added under cooling to the reaction mixture until pH 5 was reached. By-products (mainly Fc-CH_2OH) and unreacted 6-aminocaproic acid were extracted (3 times) from the reaction mixture using EtOAc. The volume of the H_2O phase was then reduced to 50 mL at 50 °C under vacuum. The brownish-yellow raw product crystallizing from this solution was re-dissolved in hot ethanol and recrystallized by slow evaporation of the solvent,

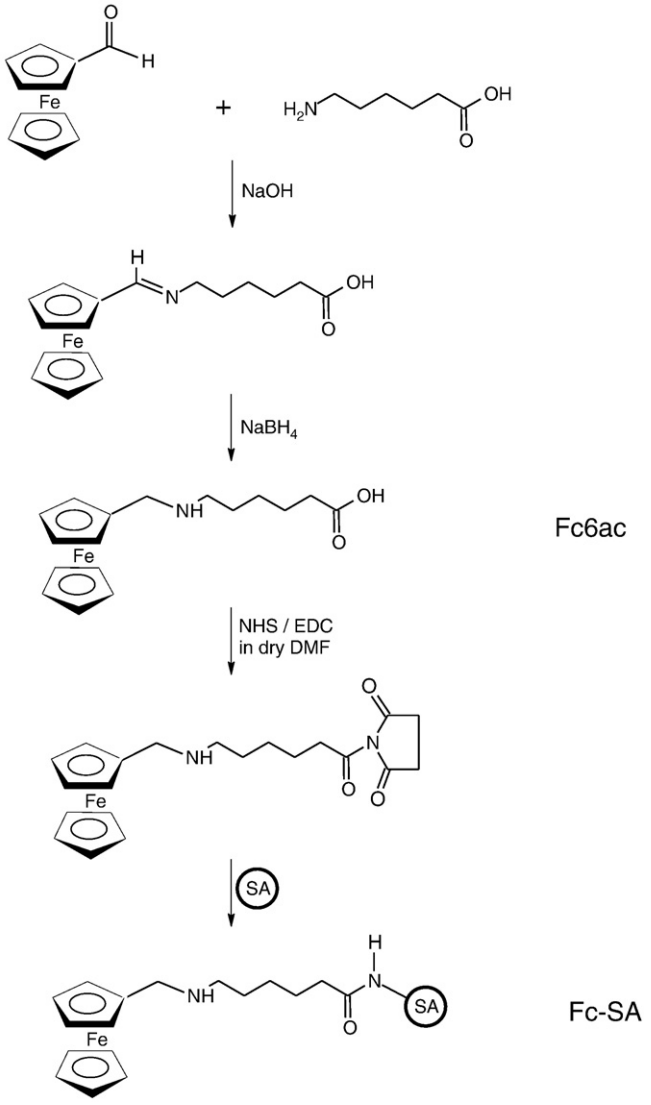

Scheme 2. Synthesis of Fc6ac and Fc-SA.

yielding platelet-shaped yellow crystals. The product was characterized using 1H NMR in deuterated methanol.

2.2.2. Ferrocene-labeled streptavidin (Fc-SA)

36 mg of [*N*-(ferrocenylmethyl)-6-amino)hexanoic acid, 14 mg *N*-hydroxysuccinimide (Fisher), and 22 mg [*N*-(3-dimethylaminopropyl)-*N*′-ethyl-carbodiimide hydrochloride] (Sigma Aldrich) in 1 mL of dry DMF were heated under N_2 atmosphere with stirring at 80 °C for 1.5 h. Nine aliquots (15 μL) of this solution were added to a solution of 2 mg of streptavidin in 1 mL of PBS buffer (0.1 M, pH 7.4). The solution was stirred overnight at room temperature with the appearance of some precipitates. The precipitates were removed by centrifugation and the supernatant was dialyzed (2 times) against 0.1 M PBS buffer (pH 7.4) to remove the unreacted ferrocene. All equipments for this synthesis were dried in the dryer at 200 °C and next were kept in a dessicator until the synthesis.

2.3. Apparatus

Cyclic voltammetry studies were performed using a potentiostat/galvanostat, ModelPS-1705 (Elchema, Potsdam, NY, U.S.A.). All voltammetric experiments were carried out in a three-electrode cell with a Pt wire as the counter electrode, a (KCl) saturated Ag/AgCl as

the reference electrode, and gold disk electrode of 1.6 mm diameter as the working electrode. The working gold disk electrode was polished before each measurement with 0.3 and, at the end, 0.05 μm diameter Al_2O_3 powders on a wet pad. After polishing, the aluminum oxide was removed by rinsing the electrode surface with a direct stream of ultrapure water (Mili-Q, Milipore, Billerica, MA, USA; conductivity of 0.056 μS/cm). In voltammetric experiments, the electrochemical cell was kept in a Faraday cage to minimize the electrical noise.

An electrochemical quartz crystal nanobalance model EQCN-700 (Elchema) with 10 MHz AT-cut quartz crystal resonators was used in the study. The EQCN technique allowed us to record simultaneously voltamperometric and nanogravimetric characteristics. The resonant frequency of the quartz crystal lattice vibrations in a thin quartz crystal wafer was measured as a function of the mass attached to the crystal interfaces. For thin rigid films, the interfacial mass change Δm is related to the shift in resonance oscillation frequency Δf of the EQCN through the Sauerbrey equation [77,80,81]:

$$\Delta f = \frac{2\Delta m n f_0^2}{A\sqrt{\mu_q \rho_q}} \quad (1)$$

where f_0 is the resonance oscillation frequency in the fundamental mode, n is the overtone number, A is the piezoelectically active surface area, ρ_q is the density of quartz ($\rho_q = 2.648\ g\ cm^{-3}$), and μ_q is the shear modulus of quartz ($\mu_q = 2.947 * 10^{11}\ g\ cm^{-1}\ s^{-2}$). The oscillator was tuned to the series resonance frequency of working piezoelectrodes to minimize effects due to energy dissipation in protein films. All experimental variables influencing the resonant frequency [77] of the EQCN electrodes such as the temperature, pressure, viscosity and density of the solution, were kept constant during measurements. The piezoelectrically active (geometrical) surface area of the working Au electrode was 0.196 cm^2 and the real surface area $A = 0.255\ cm^2$ (roughness factor $R = 1.3$). A 200 nm thick Au film was deposited on a 14-mm diameter, 0.166 mm thick AT-cut quartz resonator wafer with vacuum evaporated Ti adhesion interlayer (20 nm thick). The real surface area was determined for Au-EQCN electrodes by a standard monolayer oxide formation procedure [82]. The resonator crystals were sealed to the side opening in a glass vessel of 50 mL capacity using high purity siloxane glue with intermediate viscosity (Elchema SS-431). The seal was cured for 24 h at room temperature. The working electrode was polarized using Pt wire counter electrode and its potential measured vs. (KCl) saturated Ag/AgCl reference electrode. The measured resonance resistance change during the attachment of SA to bMUD SAM was negligible, so the observed frequency shift was assumed to be due primarily to the mass variation of the film. This enabled us to determine the surface coverage of SA and/directly related to it, suface coverage of pb-DNA.

2.4. Preparation of hybridization biosensors

Each measurement involved an immobilization/detection cycle at a freshly prepared gold disk electrode. All experiments were performed at room temperature (22 ± 1 °C). The preparation of the electrochemical DNA hybridization sensor involved several steps, including modification of the electrode surface by mixture of the thiols with MUD:bMUD = 9:1 (0.9 mM MUD and 0.1 mM bMUD), SA (0.2 mg/mL in 0.02 M PBS buffer pH 7.4), attachment of bp-DNA, hybridization with bt-DNA, Fc-SA binding, and voltammetric measurements.

2.4.1. Cleaning procedure of gold disk electrodes

The working gold disk electrode was polished with 0.3 μm Al_2O_3 powder on a wet pad. After polishing, the electrode was rinsed with a direct stream of ultrapure water (Milli-Q, Millipore, Billerica, MA, US; conductivity of 0.056 μS/cm) to remove aluminum oxide from the surface. The electrodes were electrochemically pretreated first by cycling between 0 V and 1.8 V (hold 10 s at 1.8 V) in a 0.5 M NaOH with scan rate 50 mV/s, then cycling between 0 and 1.15 V (vs. Ag/AgCl) in 0.1 M H_2SO_4 solution until a stable voltammogram typical for a clean gold electrode was observed [83].

2.4.2. Modification of gold electrode surface with binary layer of thiols

The clean bare gold electrodes were rinsed with distilled water, slowly dried with argon and immediately immersed in a 1 mM binary mixture of thiols (10% bMUD, 90% MUD at a net concentration 1 mM) in ethanolic (99.8%) solution overnight at room temperature. This composition is an optimized matrix for streptavidin binding [84]. The resulting electrode with self-assembled binary thiols was slowly rinsed with pure ethanol and water to remove physically adsorbed thiol molecules.

2.4.3. Biotin–streptavidin linkage

The streptavidin films were assembled on biotin-containing surfaces by placing of a 2 μL drop of 0.2 mg/mL SA solution in 0.02 M PBS buffer (pH 7.4) and waiting for 1 h. Then the electrode was slowly rinsed with 0.02 M PBS buffer.

2.4.4. Immobilization of bp-DNA

After these steps, a 7 μL drop containing bp-DNA (1 μM solution in 0.02 M PBS buffer, pH 7.4) was placed onto the electrode surface to form a sensing layer and the electrode was kept for 1 h under the cover. Next, the electrode was carefully rinsed with 0.02 M PBS buffer.

2.4.5. Hybridization

Onto a freshly prepared ssDNA sensor, a 7-μL drop of hybridization buffer solution (0.02 M PBS buffer, pH 7.4, with 1 M NaCl) containing a given concentration of bt-DNA was placed and the electrode was incubated for 1 h. Similar procedure was applied to test the hybridization with non-complementary and non-biotinylated sequences. Next, the electrode was carefully rinsed with 0.02 M PBS buffer.

2.4.6. Attachment of ferrocene labeled streptavidin (Fc-SA)

Fc-SA could be attached to the hybridized biotinylated complementary target DNA by placing a 2 μl drop of 40 μM Fc-SA solution in 0.1 M PBS buffer (pH 7.4) on the sensor surface and waiting for 1 h. After the accumulation of Fc-SA on a hybridized surface, the electrode was rinsed with PBS buffer to remove physically adsorbed Fc-SA molecules. The entire procedure of the sensor preparation is summarized in Scheme 3.

2.4.7. Voltammetric measurements

The electrochemical DNA-hybridization biosensors prepared in this way were immersed in the degassed pure 0.02 M PBS buffer (pH 7.4) and the cyclic voltammograms were recorded in the potential range 0 V to 0.6 V.

3. Results and discussion

3.1. Design and testing of EQCN-based DNA-hybridization biosensor

The response of the EQCN is very sensitive to the deposition of consecutive layers on the electrode surface. The multilayered surface modification is based on the affinity of streptavidin and biotin and on the hybridization process between probe and target DNA. The gold piezoelectrode was first modified with a MUD and bMUD monolayer SAM, followed by the assembly of a layer of SA via biotin–streptavidin linkages. Then the bp-DNA was attached to the streptavidin molecules. After adding the target bt-DNA to the solution, the hybridization process was carried out. In the last step, a 20 μl droplet of Fc-SA was placed on the multilayer surface architecture.

The resonant frequency shifts $-\Delta f$ (corresponding to the mass accumulation) for subsequent stages of sensory film synthesis: SA assembly, probe bp-DNA attachment, and the successive hybridization of the target bt-DNA, were: 70 ± 6 Hz, 68 ± 4 Hz, and 71 ± 5 Hz,

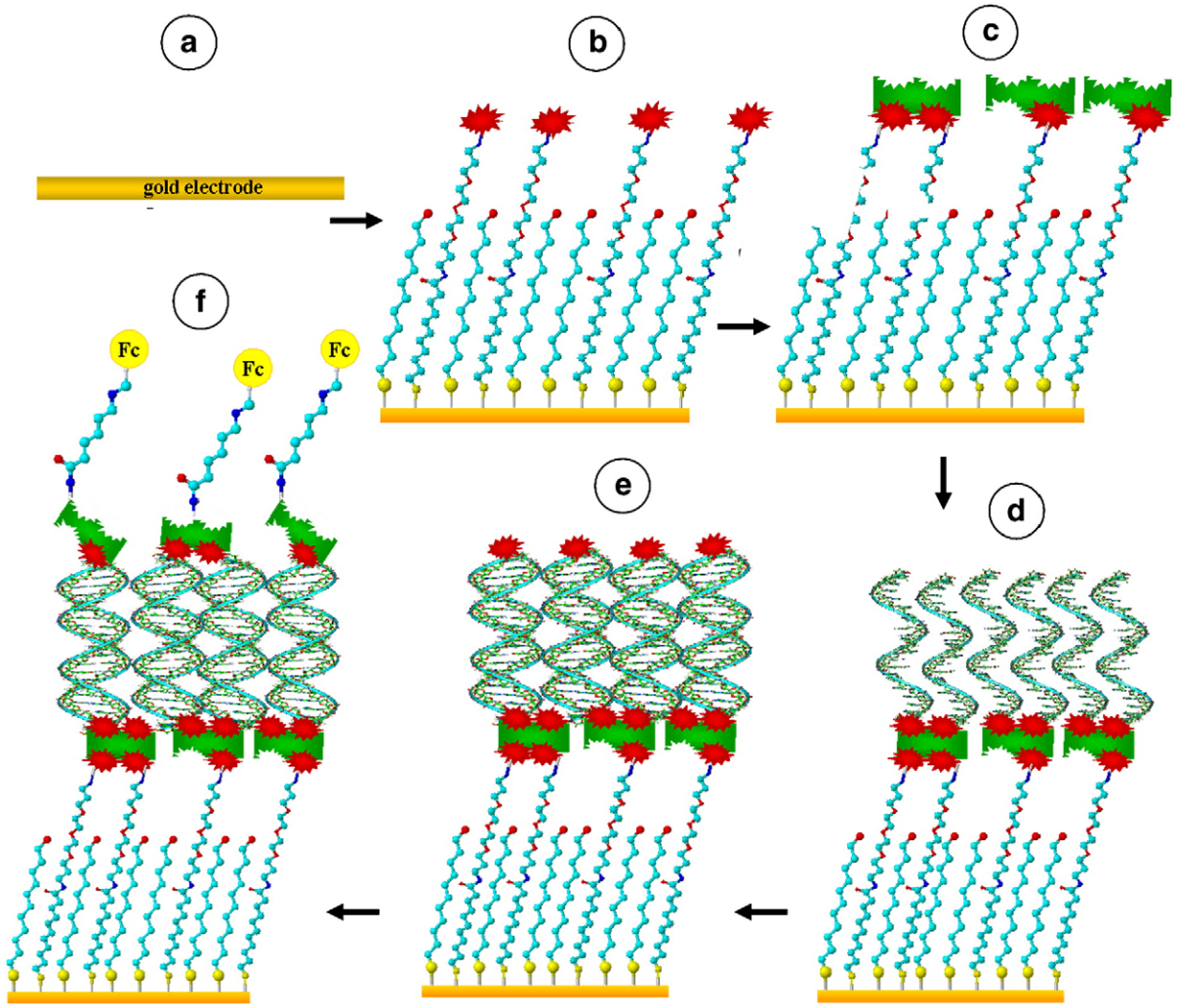

Scheme 3. Preparation of a DNA-hybridization sensor. A bare gold piezoelectrode (a), after deposition of a mixed SAM of MUD and bMUD (b), followed by attachment of streptavidin (SA) (c), and biotinylated single-stranded pb-DNA (d); the sensor was then subjected to hybridization of its pb-DNA with single-stranded target tb-DNA from solution (e) and functionalized with a layer of SA labeled with redox transducer ferrocene FC (f).

respectively, see Fig. 1. The apparent mass increase relating to the observed experimental frequency shift for streptavidin binding is: $m_{SA} = -0.8673 * 70 = 60.7$ ng/QC which corresponds to 238 ng/cm^2.

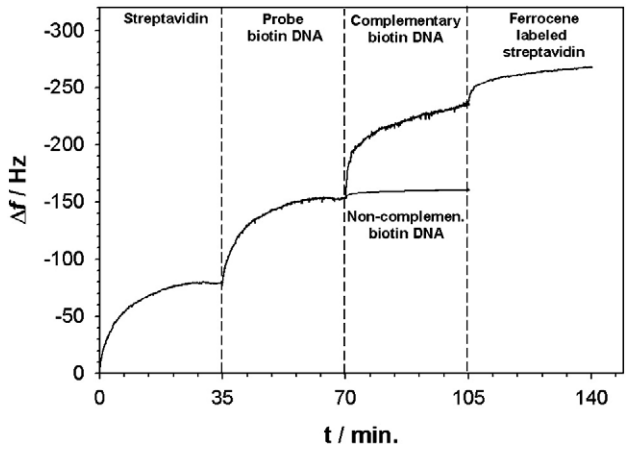

Fig. 1. Frequency shifts observed during the construction of a biosensor by deposition of subsequent layers of: SA, bp-DNA, complementary bt-DNA, and Fc-labeled SA on a biotinylated MUD-modified Au-EQCN electrode. The frequency response of the piezosensor to a non-complementary bt-DNA is also included. All solutions were prepared in 0.02 M PBS buffer (pH 7.4). The negative frequency shifts correspond to the apparent mass increases.

Hence, the molar surface concentration of SA in the layer is: $\gamma_{SA} = m_{mono}/M_{SA} = 4.51$ pmol/cm^2, where $M_{SA} = 52{,}800$ Da. This value of γ_{SA} corroborates well with actual dimensions of streptavidin tetramer (5.4 × 6.3 nm) which leads to the theoretical coverage $\gamma_{SA,theor} = 4.89$ pmol/cm^2 for a close packing 2D array. This means that the SA layer is very close to tight packing density for the maximum film functionality. The mass uptake obtained for bt-DNA is larger than expected. This is likely due to the electrolyte uptake since only two DNA strands can be attached to each SA molecule in the film. The surface concentration of bp-DNA is therefore estimated from the surface coverage of SA rather than from the Δf signal for bp-DNA deposition. Thus, $\gamma_{bpDNA} = 9.0$ pmol/cm^2. Through titrating the surface bound bp-DNA (prepared at 1 μM) with increasing concentrations of bt-DNA (1 nM to 1 μM), the Δf signal decrease (mass increase) was observed as shown in Fig. 2. A plot of plateau values of Δf from Fig. 2 vs. bt-DNA concentration, shown in Fig. 3, represents the adsorption isotherm with linear response up to 150 nM. The EQCN frequency shift decreases linearly with the concentration of complementary bt-DNA sequences in the range from 1×10^{-9} to 150×10^{-9} M. The obtained quantification limit is *ca.* 30×10^{-9} M of bt-DNA in the sample, corresponding to the presence of ~54×10^{12} copies of DNA in the solution (3 mL). This value was assumed as equal to $10\sigma_{\Delta f}$ where $\sigma_{\Delta f}$ is the standard deviation of the frequency shift measured upon addition of non-complementary bt-DNA.

The linear relationship between resonant frequency shift and concentration of bt-DNA, C_{btDNA}, can be described by the following

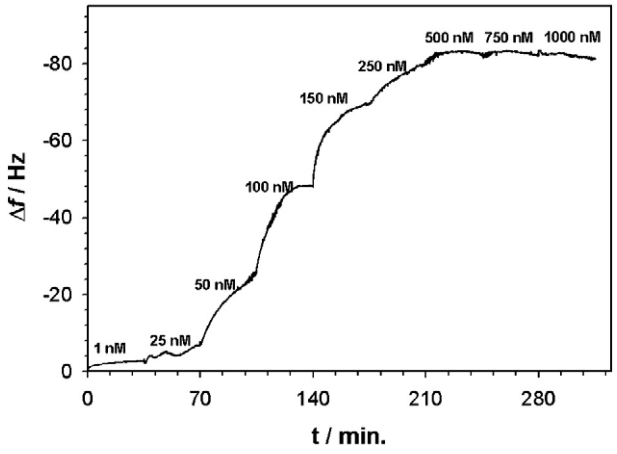

Fig. 2. Titration of a bp-DNA immobilized on a Au/bMUD/SA electrode with increasing bt-DNA concentrations, from 1 nM to 1000 nM, monitored by EQCN. The bp-DNA was deposited from a at 1 mM solution. All solutions were prepared in 0.02 M PBS buffer (pH 7.4).

formula: $-\Delta f = (0.418 \pm 0.03)C_{btDNA} + (1.94 \pm 0.5)$, r = 0.992; Δf is in Hz and C_{btDNA} in nM. From the slope of the linear portion of the curves and the instrumental noise level of the measured signal (~0.01 Hz for EQCN), the calculated signal to noise ratio is 40.

3.2. DNA-hybridization sensor with voltammetric monitoring

The DNA biosensors with redox residue attached have been explored in the context of electrocatalytic amplification of oligonucleotide hybridization by Knoll et al. [62]. The interactions of various redox couples from a solution with DNA biosensors have been studied by Abruna group [61]. In these investigations, the binding constants associated with electrostatic and intercalative interactions could be determined using voltammetric techniques.

In the electrochemical biosensor architecture developed in this work, the redox current signal of ferrocene can only appear when some of the immobilized probe DNA has hybridized to form a duplex. When hybridization occurs, the bt-DNA sequence binds to the complementary ss-DNA of the probe. Target DNA sequences have been modified with a biotin group attached to the 5′-end in order to provide link to attach a ferrocene labeled streptavidin redox transducer moiety. Four biotin molecules can bind to each streptavidin. When a non-complementary biotin labeled bt-DNA sequence is applied, the hybridization can not occur. Therefore, no contact can be made between the redox indicator and the electrode surface and no current signal can be detected. Also, no current signal would be detected if, in the hybridization step, a non-modified complementary ss-DNA sequence is used.

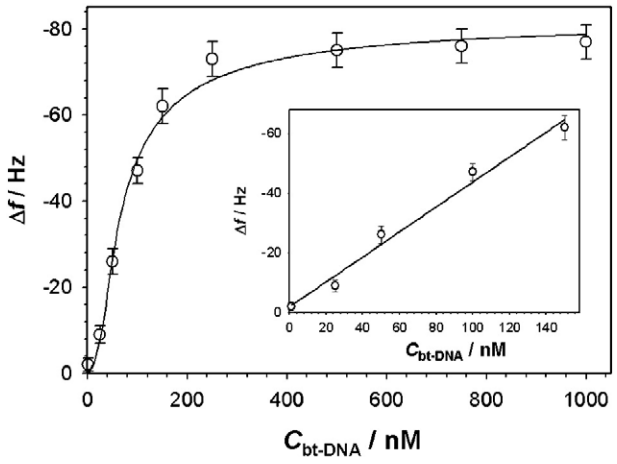

Fig. 3. Plot of EQCN frequency shifts vs. bt-DNA concentration showing saturation at higher concentration levels. Inset: Linear response up to 150 nM.

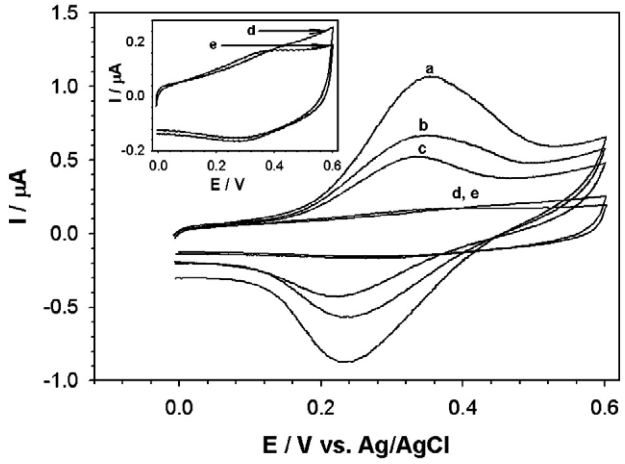

Fig. 4. Cyclic voltammograms obtained for a sensory film (Au/bMUD/SA/bp-DNA) after interaction with 1 μM of: (a) complementary bt-DNA sequence, (b) C–A mismatch complementary bt-DNA sequence, (c) C–A and G–A double-mismatch complementary bt-DNA sequence, (d) complementary non-biotinylated t-DNA sequence, and (e) non-complementary biotinylated DNA sequence. Experimental conditions: 0.02 M PBS buffer (pH 7.4), scan rate 50 mV/s, diameter of disk gold electrode 1.6 mm.

Cyclic voltammograms were recorded to determine the extent of hybridization that occurred during the interaction of the biosensor with various ss-DNA analytes. Thus, the bp-DNA sequence was exposed to both the complementary bt-DNA sequences as well as to the mismatched bt-DNA sequences: bt-DNA* and bt-DNA**, non-complementary ss-DNA, and complementary non-modified t-DNA.

The obtained results are presented in Fig. 4. Because the electron transport between Fc and electrode surface through the DNA base stack depends on the stacking of the bases in the double helix, the presence of mismatches results in lower current response. In this study, the bt-DNA* sequence with a single CA mismatch (biotin-TCGAACTATCACTGTCGAAT) and the bt-DNA** sequence with two (CA and GA) mismatches (biotin-TCGAACTATCACTATCG-AAT) were used. The corresponding

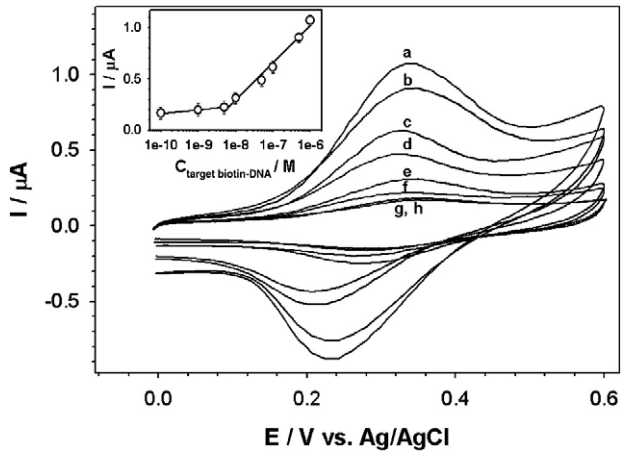

Fig. 5. Cyclic voltammograms obtained for a sensory recognition film (Au/bMUD/SA/bp-DNA) after interaction with complementary bt-DNA sequences with concentration [M]: (a) 1×10^{-6}, (b) 5×10^{-7}, (c) 1×10^{-7}, (d) 5×10^{-8}, (e) 1×10^{-8}, (f) 5×10^{-9}, (g) 1×10^{-9}, (h) 1×10^{-10}. Inset: Plot of the Fc-peak oxidation currents vs. concentration (logarithmic scale) of the complementary bt-DNA sequences in 7 μl droplets. Error bars: ± standard deviation for one electrode, one DNA delivery, 3 measurements. Experimental conditions: as in Fig. 4.

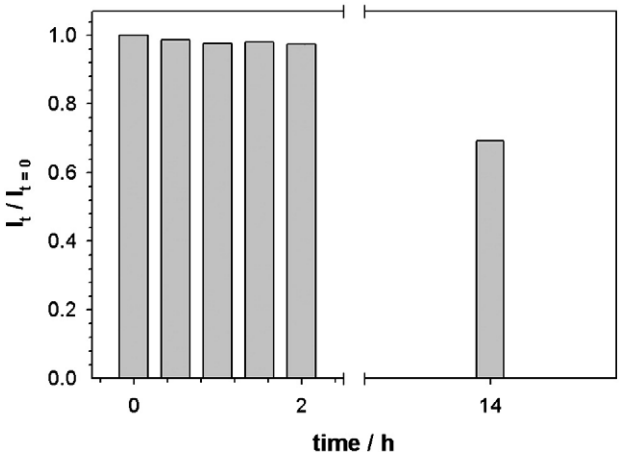

Fig. 6. Stability of the biosensor (Au/bMUD/SA/bp-DNA/bt-DNA/SA/bFc) response in time. Electrode was kept in 0.02 M PBS buffer.

voltammograms shown in Fig. 4, reveal a 38% and 52% current drop for single mismatch (CA) and double- mismatch (CA, GA), respectively. This indicates that the DNA-hybridization biosensor tagged with ferrocene-labeled streptavidin is sufficiently sensitive to detect mismatches without any extra treatment and measurement. The analytical performance of the DNA biosensor with different concentrations of target was evaluated by cyclic voltammetry. Typical voltammograms are presented in Fig. 5. The reproducibility of the measurements was satisfactory for bt-DNA concentrations in the range from 1×10^{-6} to 1×10^{-9}M. The relative standard deviation was *ca.* 10% (single electrode, 3 measurements).

The calibration curve of the Fc oxidation current vs. DNA concentration is shown in the inset of Fig. 5. The peak oxidation current varies linearly with the logarithm of concentration of complementary bt-DNA sequences, log[bt-DNA], in the range from 1×10^{-6} to 6×10^{-9}M. The obtained *quantification limit* is ca. 42 fmol (10^{-15} mol) in a 7 μl droplet and corresponds to the concentration of *ca.* 6×10^{-9}M of target DNA in the sample, equivalent to the presence of ~25×10^{9} DNA copies in the droplet. This value was determined by adding $10\sigma_i$ to the average value of baseline current (where σ_i is the standard deviation of the current measurements with non-complementary biotinylated t-DNA). The obtained *detection limit* is *ca.*7 fmol in a 7 μl droplet and corresponds to the concentration of *ca.*1×10^{-9}M of target DNA in the sample. This value was determined by adding $3\sigma_i$ to the average value of the baseline current.

The DNA sensor stability was tested for constant bt-DNA analyte concentration. In general, for a sensing film to be useful in a DNA hybridization assay, the film should be stable over at least the timeframe of the experiment (typically 1 h). The stability of the peak current response for the oxidation of ferrocene tethered to the sensory film is depicted in Fig. 6. The stability was tested by periodically measuring the voltammetric peak current. The sensor was stored in the electrolyte buffer between measurements. The current response of a particular sensor was practically unchanged during the first 2 h (with the relative standard deviation of *ca.*1%), and dropped to the level of 70% of the initial response after 14 hours.

The voltammograms presented in Fig. 5 exhibit well-defined oxidation and reduction peaks corresponding to the Fc/Fc^{+} redox couple. The peak currents scale linearly with the scan rate indicating surface confined electroactive species, as expected. The separation of peaks increases with the scan rate. For the low scan rates, $v\leq20$ mV/s, $\Delta E_p = 60$ mV and for $v = 500$ mV/s, $\Delta E_p = 294$ mV.

3.3. Determination of DNA damage due to Cr(VI) using DNA biosensor

Cr(VI) has been established as a human carcinogen. The reaction of Cr (VI) with DNA creates a number of putative lesions in cellular systems including inter- and intrastrand cross-linked adducts, DNA-protein cross-links, DNA strand breaks, abasic sites, and oxidized nucleic acid bases [85–87]. The oxidative damage (including the formation of oxidized lesions in DNA) is considered one of the critical steps in the induction of carcinogenesis by Cr(VI). The DNA-strand breaks are formed when the oxidation of DNA occurs at the deoxyribose sugar. The DNA oxidations can also occur at the nucleic acid bases forming oxidized base lesions [88,89].

We have investigated the DNA damage caused by Cr(VI) species using the DNA hybridization sensor developed in this work. In the tests performed, the sensor was immersed in the solution containing the appropriate amount of the toxicant. After 5 min of immersion in 50 μM solutions of Cr(VI), the biosensor was rinsed, immersed in 0.02 M PBS buffer (pH 7.4) and cyclic voltammetry was quickly carried out to evaluate the sensor response. Then, the sensor was washed and subjected for the next 5 min period in the toxic solution under test and so on. It is seen from Fig. 7 that the subsequent exposures to 50 μM CrO_4^{2-} alone cause considerable damage to DNA manifested by a substantial decrease in the sensor signal. The DNA damage φ_{DNA} measured as the relative current decrease of the DNA sensor:

$$\varphi_{DNA} = (I_{t=0} - I_t) / I_{t=0} \quad (2)$$

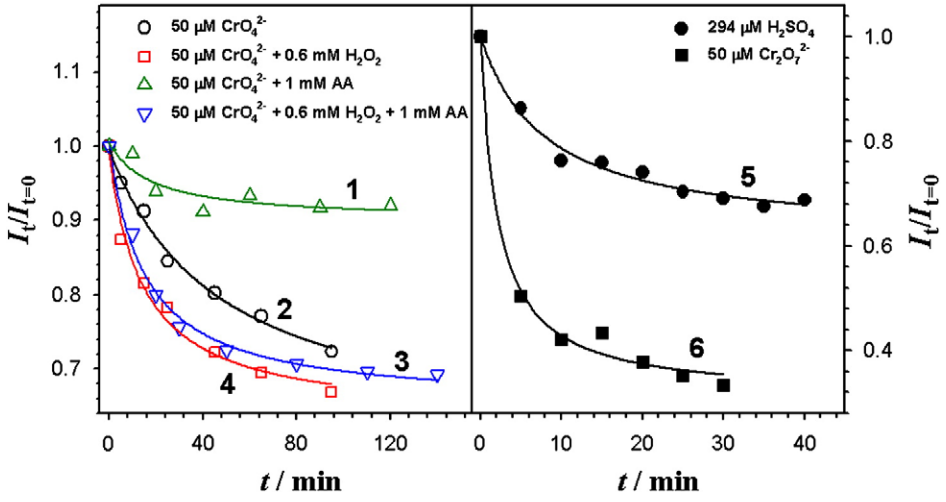

Fig. 7. Effects of Cr(VI) species on the current response of a Au/bMUD/SA/b-dsDNA/SA/Fc biosensor. Experimental conditions: $v = 50$ mV/s, 0.02 M PBS buffer (pH 7.4).

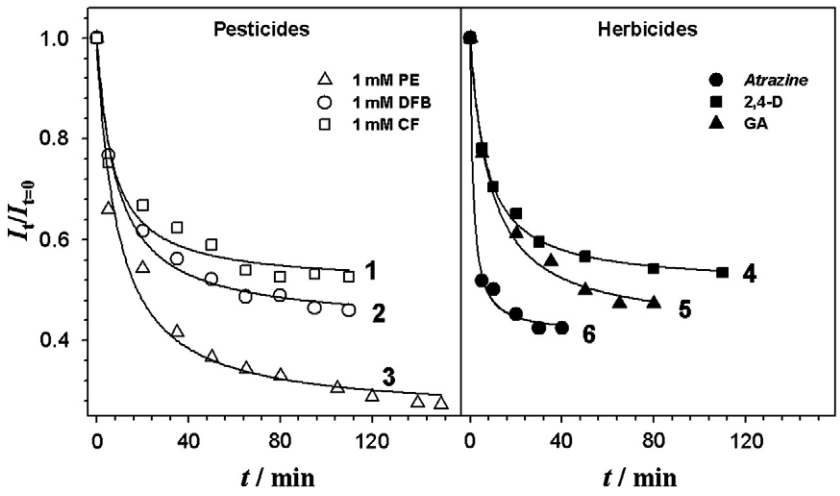

Fig. 8. Effects of various pesticide and herbicide species on the current response of a Au/bMUD/SA/b-dsDNA/SA/Fc biosensor. Experimental conditions: $v = 50$ mV/s; 0.02 M PBS buffer (pH 7.4); PE: paraoxon-ethyl; DFB: diflubenzuron; CF: carbofuran; 2,4-D: 2,4-dichlorophenoxyacetic acid; GA: glufosinate ammonium.

approached 0.28 in 90 min of the biosensor contact with 50 μM CrO_4^{2-} solution. The addition of 1 mM ascorbic acid effectively prevents the DNA damage due to the reduction of CrO_4^{2-} in solution and so φ_{DNA} is low: $\varphi_{DNA} = 0.08$. Contrary, the H_2O_2 (0.6 mM) added to the CrO_4^{2-} solution acts synergistically and increases the DNA damage done by CrO_4^{2-}: $\varphi_{DNA} = 0.34$. The addition of AA to the $CrO_4^{2-} + H_2O_2$ solution does not prevent DNA from damage and $\varphi_{DNA} = 0.31$ is observed. Among chromium species, $Cr_2O_7^{2-}$ has shown the strongest effect on DNA biosensor with the Fc oxidation current decreased by more than 68% ($\varphi_{DNA} = 0.68$) in 30 min of the biosensor contact with 50 μM $Cr_2O_7^{2-}$ solution. On the contrary, CrO_4^{2-} caused only 28% diminution of the Fc oxidation current. Since in the $Cr_2O_7^{2-}$ molecule, there are two chromium species at hexavalent state, the observed effect should be twice as strong as that for CrO_4^{2-}, if both chromium atoms were active in the DNA oxidation. The effect of the supporting sulfuric acid alone was also tested because in experiments with bichromates a strongly acidic medium must be maintained to sustain the bichromates in the solution. As seen from Fig. 7, the acid alone caused much less damage to the DNA sensor ($\varphi_{DNA} = 0.32$). Assuming that the action of bichromate and sulfuric acid are additive, one would have for the DNA damage by bichromates alone: $\varphi_{DNA} = 0.67 - 0.32 = 0.35$, which is higher than damage done by CrO_4^{2-} alone but not twice as high. Because the Cr(VI) species cause DNA damages such as the strand breaks and the oxidation of nucleic-acid bases, these changes in DNA structure must have the influence on the electron transport between ferrocene and the electrode surface through the DNA double helix. The DNA hybridization sensor developed in this work has shown remarkable sensitivity to DNA damage inflicted by the short time interactions with Cr(VI) species.

3.4. Application of DNA biosensor to comparative analysis of DNA damage caused by herbicides and pesticides

Herbicides and pesticides belong to the most unwanted environmental pollutants. They have a high acute toxicity and a wide range of biological activities. We have examined the DNA damage and structural alterations, such as the double-helix unwinding, caused by various herbicides and pesticides using the DNA biosensor developed in this work. We have investigated known herbicides (atrazine, 2,4-D, and glufosinate ammonium) and representative compounds from the main groups of pesticides, including organophosphate, carbamate, and urea pesticides, *viz.* paraoxon-ethyl (PE), diflubezuran (DFB), and carbofuran (CF). The methodology involved was similar to the one applied in the study of DNA damage by chromium species.

Freshly prepared biosensors were immersed in 1 mM solution of each herbicide/pesticide for a predetermined time, followed by rinsing and immersing in pure PBS buffer solution. The DNA damage was evaluated by voltammetric measurements in PBS buffer. The obtained results are presented in Fig. 8. It is seen that the most negative influence on DNA hybridization among herbicides has atrazine for which the DNA damage φ_{DNA} approached 0.58. For other herbicides tested, $\varphi_{DNA} = 0.47$ for 2,4-D and $\varphi_{DNA} = 0.52$ for GA. Among pesticides tested, CF caused the least damage ($\varphi_{DNA} = 0.48$), followed by DFB ($\varphi_{DNA} = 0.54$) and PE ($\varphi_{DNA} = 0.72$). Therefore, the most severe DNA damage, as tested by the DNA-hybridization sensor, among all herbicides and pesticides examined in this work has been observed for the herbicide atrazine and the organophosphate pesticide, paraoxon-ethyl. The compounds tested can bind to DNA non-covalently or covalently and have been implicated in the formation of breaks in the DNA strands and/or DNA unwinding.

The herbicide atrazine is one of the most heavily used herbicides in the United States. Atrazine exhibits endocrine disruptor activity [4]. There is evidence that it interferes with the reproduction and development of cells [3–5,7,11,15], and may cause cancer [6,8–10,13]. The experiments described above have shown that atrazine causes considerable changes in DNA leading to the reduction of the charge transport between the electrode surface and the redox centers. This measurement is so sensitive because just one obstacle on the way of charge transport path through a

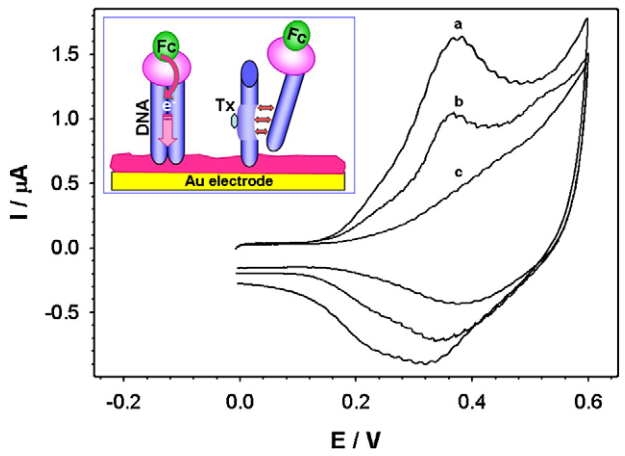

Fig. 9. Cyclic voltammograms obtained for a Au/bMUD/SA/b-dsDNA/SA/Fc biosensor before (a) and after immersing the biosensor in: 0.1 mM (b), and 1 mM atrazine solution (c) for 1 h. Conditions: $v = 50$ mV/s; 0.02 M PBS buffer (pH 7.4). Inset: schematic view of the conducting DNA duplex and damaged non-conducting DNA strand.

DNA channel affects electrical conductance through this channel. While atrazine may also bind non-specifically to streptavidin, this binding will not influence the electrical conductance. The non-specific binding of atrazine to streptavidin in sensory film is also not a major factor since atrazine has been found to bind rather weekly to proteins [90], especially at low concentrations (for instance, the association constant for atrazine binding to human serum albumin is $K_b = 3.50 \times 10^4\ M^{-1}$). The independent tests with piezosensors lacking DNA (i.e., Au/bMUD/SA) have shown resonant frequency shifts of less than 1 Hz upon exposure to atrazine. Moreover, in the presence of DNA attached to SA in sensory films, a large part of streptavidin surface is blocked by DNA and, hence, atrazine has less access to SA to interact with these molecules. The interaction of atrazine with DNA leads to the formation of an adduct and, in consequence, to structural changes in DNA double helix. The decrease in the Fc oxidation current observed in voltammetric experiments (Fig. 9) confirms the changes in the biosensor response. They show the diminution of the Fc redox signal corroborating that the communication between the Fc moiety and the electrode surface through a DNA double-helix is affected. Since the redox probe current does not decrease to zero, we conclude that atrazine does not damage DNA through the formation of breaks, which could destroy the DNA hybridization and could result in complete current cessation, but rather acts as to cause an unwinding of the DNA, thereby decreasing the film conductance. In view of the rather weak interactions of atrazine with proteins, it is highly unlikely that atrazine could possibly disrupt the strong binding SA-bpDNA for which the binding constant is some 12-orders of magnitude higher than that anticipated for atrazine-SA.

3.5. Kinetics of DNA damage and unwinding

The transients recorded for toxicant-induced DNA damage and unwinding recorded for all toxicants investigated show redox current decays. To elucidate the mechanism of a toxicant interaction with DNA, we have evaluated first the limiting rate of mass transport for the substrate of the process, the toxicant Tx. For the semi-infinite mass transport in the solution, outside of the film, the diffusion-controlled mass transport can support fast heterogeneous processes up to the Cottrell rate of the mass transport v given by:

$$v = \frac{C_{Tx} D}{\sqrt{\pi D t}} \tag{3}$$

where C_{Tx} is the Tx concentration, D its diffusion coefficient, and t is the interaction time. Assuming the experimental value: $C_{Tx} = 1 \times 10^{-6}$ mol/cm^3 (1 mM) and typical diffusivity in solution $D = 1 \times 10^{-5}$ cm^2/s, one obtains for $t = 60$ s a value $v = 230\ \mu mol\ s^{-1}\ cm^{-2}$ This means that in 1 s this limiting mass flux can deliver 230 μmol of Tx per cm^2, which is orders of magnitude higher than the actual surface concentration of DNA double-helices, $C_{s,DNA} = 4.5$ pmol/cm^2. While the limiting mass flux decreases with time, the natural convection which takes over at longer times, approximately $t > 100$ s, provides more than the sufficient amount of the substrate for the reaction with DNA in the sensory film. Therefore, it becomes clear that the interactions of toxicants are slow processes which are not controlled by mass transport in bulk solution. The mass transport within the film requires a separate consideration. Here, we have a layer of nearly vertical DNA double-helices and the toxicant diffusion proceeds mainly in the free (solution) space between DNA columns. In order to evaluate the rate of diffusion in the film, it is necessary to determine first the amount of free diffusional space. In a tight space, the mass transport rate may be limited. The relative cross-sectional area taken up by DNA columns can be expressed as the DNA coverage θ given by:

$$\theta = \frac{C_{s,DNA} N_A S_{DNA}}{S_{tot}} \tag{4}$$

where S_{DNA} is the cross-sectional area of a single DNA double-helix, C_s is the surface concentration of DNA, N_A is the Avogadro number, and S_{tot} is the total area of the electrode. Introducing values for $C_{s,DNA} = 4.5$ pmol/cm^2 and $S_{DNA} = \pi(d/2)^2 = 3.46$ nm^2 where $d = 2.1$ nm is the diameter of the DNA double-helix, one obtains: $\theta = 0.093$. This is a relatively low surface coverage which can not cause any considerable blocking effect for the mass transport. From the diffusion layer thickness model, we have:

$$h = \sqrt{\pi D t} \tag{5}$$

where h is the layer thickness. On the basis of this expression, the diffusional time constant τ_D for the mass transport in the free solution space along DNA columns with height h is obtained:

$$\tau_D = \frac{h^2}{\pi D} \tag{6}$$

By introducing $h = 5.4$ nm for the length of 20 bp DNA strands, one obtains $\tau_D = 9.3 \times 10^{-9}$ s, a very fast mass transport indeed. Therefore, no transport limitations are expected for both the semi-infinite diffusion outside the film and also for the solution transport inside the film. The experimental transients presented in Figs. 7 and 8 represent then kinetically-controlled processes. Assuming simple first order reaction kinetics, one can estimate time constants for all these processes:

$$v = v_0 \exp\left\{-\frac{t}{\tau_k}\right\} \tag{7}$$

The values of τ_k obtained range from 1.2×10^3 to 4.8×10^3 s, pointing to a very slow kinetic regime. If only a simple adduct of a given toxicant to the DNA strand were formed, the reaction kinetics would be faster. Therefore, it is reasonable to assume that conformational transformation of DNA is occurring during its interaction with the toxicant. This conformation change likely includes breaking hydrogen bonds between nucleotides forming base pairs and interrupting the base stacking [91–97]. From the viewpoint of energy required to break hydrogen bonds and interrupt base stacking, there are considerable differences between H-bond energies for base pairs: A...T and G...C (where "..." denotes double or triple H-bonding). The energies of stacking interactions between A and T and between G and C are also different. While the energy of H-bonding for G...C is low, the H-bonding for A...T is actually destabilizing the DNA double-helix [93]. Therefore, in the reaction pathway, breaking the H-bonding of A...T would not require any energy expense. However, in order to separate one AT base pair, the distance between nucleotides forming neighbor base pairs should also be increased which could require some energy expense unless the neighbor pairs are also AT. Thus, for the bp-DNA sequence used in this work, 5′biotin-ATTCGACAGGGATAGTTCGA-3′, there are two spots of triple base pairs A...T: one attached to biotin, in positions 1–3 (the nucleotide sequence -ATT-) and one in positions 12–14 (sequence: -ATA-). There is also one spot of double A...T pairs at positions 16–17 (sequence -TT-). Hence, the easiest double-helix unwinding induced by the interaction with toxicants is at position 1–3 and 12–14 where breaking hydrogen bonds could occur without any additional energy expense. The energy expense is however, required to interrupt the stacking interactions between nucleotides in each DNA strand. Any DNA unwinding requires at least some adjustments in the angles between stacking nucleotides which will take up energy. For the same angle change $\Delta\phi$, the energy input ΔE is proportional to the stacking interaction energy:

$$\Delta E \sim -\Delta\phi \Delta G_{st,n} \tag{8}$$

where $\Delta G_{st,n}$ is the stacking free energy for the given stacking nucleotide interaction and is equal to $\Delta G_{st,a}$ or $\Delta G_{st,g}$ where

$$\Delta G_{st,a} = \frac{1}{3}\sum_i \Delta G_{st,i} \tag{9}$$

with i = AA, AT, TT and:

$$\Delta G_{st,g} = \frac{1}{3}\sum_j \Delta G_{st,j} \quad (10)$$

with j = GG, GC, CC.

In general, $\Delta G_{st,a} > \Delta G_{st,g}$. According to Yakovchuk et al. [93], $\Delta G_{st,a} = -0.92$ kcal/mol in 15 mM NaCl solution at 37 °C and $\Delta G_{st,g} = -1.44$ kcal/mol under the same conditions. This points to positions between nucleotides 1–2, 2–3, 12–13 and 13–14 in the bp-DNA sequence as most likely spots for an interruption of DNA duplex in the interaction with a toxicant. The spots 1–3 and 12–14 have already been selected for the weakness in the H-bonding. The attack of toxicants at these positions can be facilitated by the DNA breathing [98,99] which may expose the weakest spots in the duplex to the disruptive interactions with a toxicant. The stacked–unstacked equilibria in DNA duplexes have been recently characterized by Protozanova et al. [100].

The through-chain electrical conductance of DNA films depends strongly on the integrity of DNA strands. While both the unstacking and partial unwinding will cause the redox current decrease, greater effects are expected for unstacking since a single unstacking in DNA strand will cause a complete shut down of the current through that strand. It also increases the chance of dehybridization and removal of the redox moiety from the electrode surface. In the case of unstacking, the sensor redox current is proportional to the number of damaged strands:

$$I = I_0\left(1 - \frac{\Gamma_{unstack}}{\Gamma_{DNA}}\right) \quad (11)$$

where $\Gamma_{unstack}$ is the surface concentration damaged DNA strands with unstacked nucleotides, Γ_{DNA} is the total surface concentration of DNA duplexes, and I_0 is the sensor redox-signal in the absence of any damage. The detailed differences between the electrical conductance of DNA strands damaged in different ways by toxicants are not yet known. Further studies are carried out to evaluate temperature dependence of the conductance and the level of damage for different nucleotide sequences.

4. Conclusions

The DNA-hybridization biosensors developed in this work provide a sensing platform for the detections of single mismatches in the probe-target ssDNA sequences. The sensors utilize nanogravimetric and voltammetric transduction techniques. The voltammetric transduction was achieved by coupling Ferrocene moiety to streptavidin linked to biotinylated t-DNA and the mass-related frequency transduction was implemented by immobilizing the sensory p-DNA on a gold-coated quartz crystal piezoresonators oscillating in the 10 MHz shear mode. The high sensitivity of these sensors enabled us to study DNA damage and structural alteration caused by representative toxicants and environmental pollutants, including Cr(VI) species, common pesticides and herbicides. We have found that the sensor responds rapidly to any damage caused by Cr(VI) species. More severe DNA damage was observed for $Cr_2O_7^{2-}$ as compared to CrO_4^{2-}. The DNA damage caused by Cr (VI) can be prevented by adding ascorbic acid to the solution. On the other hand, the damage is increased in the presence of H_2O_2. All herbicides and pesticides examined caused DNA damage or alteration. Among these compounds, atrazine and paraoxon-ethyl caused the fastest and most severe damage to DNA. The DNA damage can be quantified using relative signal change of the sensor. The voltammetric and nanogravimetric DNA biosensors developed in this work can be applied in systematic studies of toxicity and DNA damage caused by various compounds. With further developments and automatic fabrication, the cost and reliability can be further improved so that this kind of testing can be applied in laboratory and even in the field-testing provided that portable instrumentation is available.

The methodology used here to test for DNA damage can also be employed as a simple protocol to obtain rapid comparative data concerning DNA damage caused by herbicide, pesticides and other toxic pollutants. The DNA biosensor developed in this work can, therefore, be utilized as a rapid screening device for classifying environmental pollutants and to evaluate DNA damage induced by these compounds. Further studies are being conducted to develop diagnostic tools enabling one to distinguish different kinds of DNA damage done by toxicants.

Acknowledgements

This work was supported by the DoD Grant Program Idea No. AS-073218. The Authors are indebted to Dr. Tony Molinero and Dr. Martin Walker for their help with organic syntheses and 1H NMR characterization of the products.

References

[1] I. Palchetti, A. Cagnini, M. Del Carlo, C. Coppi, M. Mascini, A.P.F. Turner, Determination of anticholinesterase pesticides in real samples using a disposable biosensor, Anal. Chim. Acta 337 (1997) 315–321.
[2] M. Del Carlo, M. Mascini, A. Pepe, G. Diletti, D. Compagnone, Screening of food samples for carbamate and organophosphate pesticides using an electrochemical bioassay, Food Chem. 84 (2004) 651–656.
[3] J. Ashby, H. Tinwell, J. Stevens, T. Pastoor, G.B. Breckenridge, The effects of atrazine on the sexual maturation of female rats, Regul. Toxicol. Pharmacol. 35 (2002) 468–473.
[4] A.R. Greenlae, T.M. Ellis, R.L. Berg, Low-dose agrochemicals and lawn-care pesticides induce developmental toxicity in murine preimplantation embryos, Environ. Health Perspect. 112 (2004) 703–709.
[5] C. Clements, S. Raph, M. Petras, Genotoxicity of selected herbicides in *Rana catesbeiana* tadpoles using alkaline single-cell gel DNA electrophoresis (comet) assay, Environ. Mol. Mutagen. 29 (1997) 277–288.
[6] L.F. Meisner, B.D. Roloff, D.A. Belluck, In vitro effects of N-nitrosoatrazine on chromosome breakage, Arch. Environ. Contam. Toxicol. 24 (1993) 108–112.
[7] J.L. Freeman, A.L. Rayburn, In vivo genotoxicity of atrazine to anuran larvae, Mutat. Res. 560 (2004) 69–78.
[8] M.C.R. Alavanja, C. Samanic, M. Dosemeci, J. Lubin, R. Tarone, C.F. Lynch, C. Knott, J.A. Hopin, J. Barker, J. Coble, D.P. Sandler, A. Blair, Use of agricultural pesticides and prostate cancer risk in the Agricultural Health Study cohort, Am. J. Epidemiol. 157 (2003) 800–814.
[9] J.C. Schroeder, A.F. Olshan, R. Baric, G.A. Dent, C.R. Weinberg, B. Yount, J.R. Cerhan, C.F. Lynch, L.M. Schuman, P.E. Tolbert, N. Rothman, K.P. Cantor, A. Blair, Agricultural risk factors for t(14;18) subtypes of non-Hodgkin's lymphoma, Epidemiology 12 (2001) 701–709.
[10] C. Hopenhayn-Rich, M.L. Stump, S.R. Browning, Regional assessment of atrazine exposure and incidence of breast and ovarian cancers in Kentucky, Arch. Environ. Contam. Toxicol. 42 (2002) 127–136.
[11] C.D. Croce, E. Morichetti, L. Intorre, G. Soldani, S. Bertini, G. Bronzetti, Biochemical and genetic interactions of two commercial pesticides with the monooxygenase system and chlorophyllin, J. Environ. Pathol. Toxicol. Oncol. 15 (1996) 21–28.
[12] Environmental Health Criteria, WHO (World Health Organization), Geneva, 1986.
[13] G. Ribas, G. Ferenzilli, R. Barale, R. Marcos, Herbicide induced DNA damage in human lymphocytes evaluated by single-cell gel electrophoresis (SCGE) assay, Mutat. Res. 344 (1995) 41–54.
[14] J. Surralles, J. Catalan, A. Creus, H. Norppa, N. Xamena, R. Marcos, Micronuclei induced by alachlor, mitomycin-C and vinblastine in human lymphocytes: presence of centromeres and kinetochores and influence of staining technique, Mutagenesis 10 (1995) 417–423.
[15] W. Fan, T. Yanase, H. Morinaga, Atrazine-induced aromatase expression is SF-1 dependent: implications for endocrine disruption in wildlife and reproductive cancers in humans, Environ. Health Perspect. 115 (2007) 720–727.
[16] D. Zeljezic, V. Garaj-Vrhovac, P. Perkovic, Evaluation of DNA damage induced by atrazine and atrazine-based herbicide in human lymphocytes in vitro using a comet and DNA diffusion assay, Toxicol. In Vitro 20 (2006) 923–935.
[17] J. Pribyl, M. Hepel, J. Halamek, P. Skladal, Development of piezoelectric immunosensors for competitive and direct determination of atrazine, Sens. Actuators B 91 (2003) 333–341.
[18] J. Halamek, M. Hepel, P. Skladal, Investigation of highly sensitive piezoelectric immunosensors for 2, 4-dichlorophenoxyacetic acid, Biosens. Bioelectron. 16 (2001) 253–260.
[19] S. Helali, C. Matelet, A. Abdelghani, M.A. Maaref, N. Jaffrezic-Renault, A disposable immunomagnetic electrochemical sensor based on functionalized magnetic beads on gold surface for the detection of atrazine, Electrochim. Acta 51 (2006) 5182–5186.
[20] M. Pohanka, P. Skládal, Electrochemical biosensors — principles and applications, J. Appl. Biomed. 6 (2008) 57–64.
[21] P. Skládal, Piezoelectric quartz crystal sensors applied for bioanalytical assays and characterization of affinity interactions, J. Braz. Chem. Soc. 14 (2003) 491–502.
[22] J.-L. Marty, B. Leca, T. Noguer, Biosensors for the detection of pesticides, Analusis 26 (1998) M144–M149.

[23] A. Ferencova, M. Adamovski, P. Grundler, J. Zima, J. Barek, J. Mattusch, R. Wennrich, J. Labuda, Interaction of tin(II) and arsenic(III) with DNA at the nanostructure film modified electrodes, Bioelectrochemistry 71 (2007) 33–37.
[24] J. Galandova, R. Ovadekova, A. Ferancova, J. Labuda, Disposable DNA biosensor with the carbon nanotubes-polyethyleneimine interface at a screen-printed carbon electrode for tests of DNA layer damage by quinazolines, Anal. Bioanal. Chem. 394 (2009) 855–861.
[25] T. Hianik, DNA/RNA aptamers — novel recognition structures in biosensing, Elsevier, Amsterdam, 2007.
[26] I.I.S. Lim, U. Chandrachud, L. Wang, S. Gal, C.J. Zhong, Assembly–disassembly of DNAs and gold nanoparticles: a strategy of intervention based on oligonucleotides and restriction enzymes, Anal. Chem. 80 (2008) 6038–6044.
[27] C.A. Mirkin, R.L. Letzinger, R.C. Mucic, J.J. Storhoff, A DNA-based method for rationally assembling nanoparticles into macroscopic materials, Nature 382 (1996) 607–609.
[28] K.M. Millan, S.R. Mikkelsen, Sequence-selective biosensor for DNA based on electroactive hybridization indicators, Anal. Chem. 65 (1993) 2317–2323.
[29] E.K. Wilson, D.N.A. Instant, detection, Chem. Eng. News 76 (1998) 47–49.
[30] M. Stobiecka, J.M. Cieśla, B. Janowska, B. Tudek, H. Radecka, Piezoelectric sensor for determination of genetically modified soybean Roundup Ready ⊘ in samples not amplified by PCR, Sensors 7 (2007) 1462–1479.
[31] A.M. Oliveira-Brett, T.R.A. Macedo, R. Raimundo, M.H. Marques, S.H.P. Serrano, Voltammetric behaviour of mitoxantrone at a DNA-biosensor, Biosens. Bioelectron. 13 (1998) 861–867.
[32] C. dos Santos Riccardi, K. Dahmouche, C.V. Santilli, P. Inácio da Costa, H. Yamanaka, Immobilization of streptavidin in sol-gel films: application on the diagnosis of hepatitis C virus, Talanta 70 (2006) 637–643.
[33] E. Katz, I. Willner, Probing biomolecular interactions at conductive and semiconductive surfaces by impedance spectroscopy: routes to impedimetric immunosensors, DNA-sensors, and enzyme biosensors, Electroanalysis 15 (2003) 913–947.
[34] R. Miranda-Castro, P. De-Los-Santos-Alvarez, J. Lobo-Castanon, A. Miranda-Ordieres, P. Tunon-Blanco, Hairpin-DNA probe for enzyme-amplified electrochemical detection of Legionella pneumophila, Anal. Chem. 79 (2007) 4050–4055.
[35] A. Erdem, M.I. Pividori, A. Lermo, A. Bonanni, M. del Valle, S. Alegret, Genomagnetic assay based on label-free electrochemical detection using magneto-composite electrodes, Sens. Actuators B 114 (2006) 591–598.
[36] Z. Chang, M. Chen, H. Fan, K. Zhao, S. Zhuang, P. He, Y. Fang, Multilayer membranes via layer-by-layer deposition of PDDA and DNA with Au nanoparticles as tags for DNA biosensing, Electrochim. Acta 53 (2008) 2939–2945.
[37] L. Song, S. Ahn, D.R. Walt, Fiber-optic microsphere-based arrays for multiplexed biological warfare agent detection, Anal. Chem. 78 (2006) 1023–1033.
[38] X. Su, Y.J. Wu, W. Knoll, Biosens. Bioelectron. 21 (2005) 719–726.
[39] F. Patolsky, A. Lichtenstein, I. Willner, Electronic transduction of DNA sensing processes on surfaces: amplification of DNA detection and analysis of single-base mismatches by tagged liposomes, J. Am. Chem. Soc. 123 (2001) 5194–5205.
[40] S.L. Pan, L. Rothberg, Chemical control of electrode functionalization for detection of DNA hybridization by electrochemical impedance spectroscopy, Langmuir 21 (2005) 1022–1027.
[41] X.H. Fang, X.J. Liu, S. Schuster, W.H. Tan, Designing a novel molecular beacon for surface-immobilized DNA hybridization studies, J. Am .Chem. Soc. 121 (1999) 2921–2922.
[42] L.M. Shamansky, C.B. Davis, J.K. Stuart, W.G. Kuhr, Immobilization and detection of DNA on microfluidic chips, Talanta 55 (2001) 909–918.
[43] N. Gajovic-Eichelmann, E. Ehrentreich-Foster, F.F. Bier, Directed immobilization of nucleic acids at ultramicroelectrodes using a novel electro-deposited polymer, Biosens. Bioelectron. 19 (2003) 417–422.
[44] V.H. Pe´rez-Luna, M.J. O'Brien, K.A. Opperman, P.D. Hampton, G.P. Lo´pez, L.A. Klumb, P.S. Stayton, Molecular recognition between genetically engineered streptavidin and surface-bound biotin, J. Am. Chem. Soc. 121 (1999) 6469–6478.
[45] P. Vermette, T. Gengenbach, U. Divisekera, P.A. Kambouris, H.J. Griesser and L. Meagher, Immobilization and surface characterization of NeutrAvidin biotin-binding protein on different hydrogel interlayers, J. Colloid. Interface Sci. 259 (259) 13.
[46] W.A. Hendrickson, A. Pähler, J.L. Smith, Y. Satow, E.A. Merritt, R.P. Phizackerley, Crystal structure of core streptavidin determined from multiwavelength anomalous diffraction of synchrotron radiation, Proc. Natl. Acad. Sci. USA 86 (1989) 2190–2194.
[47] M. Dequaire, C. Degrand, B. Limoges, Biotinylation of screen-printed carbon electrodes through the electrochemical reduction of the diazonium salt of p-aminobenzoyl biocytin, J. Am. Chem. Soc. 121 (1999) 6946–6947.
[48] O. Azzaroni, M. Álvarez, M. Mir, B. Yameen, W. Knoll, Redox mediation and electron transfer through supramolecular arrays of ferrocene-labeled streptavidin on biotinylated gold electrodes, J. Phys. Chem. C 112 (2008) 15850–15859.
[49] E.A. Bayer, S. Ehrlich-Rogozinski, M. Wilchek, Sodium dodecyl sulfate-polyacrylamide gel electrophoretic method for assessing the quaternary state and comparative thermostability of avidin and streptavidin, Electrophoresis 17 (1996) 1319–1324.
[50] G.E. McManis, R.M. Nielson, A. Gochev, M.J. Weaver, Solvent dynamical effects in electron transfer: evaluation of electronic matrix coupling elements for metallocene self-exchange reactions, J. Am. Chem. Soc. 111 (1989) 5533–5541.
[51] B. Shoham, Y. Migron, A. Riklin, I. Willner, B. Tartakovsky, A bilirubin biosensor based on a multilayer network enzyme electrode, Biosens. Bioelectron. 10 (1995) 341–352.
[52] C. Padeste, A. Grubelnik, L. Tiefenauer, Ferrocene–avidin conjugates for bioelectrochemical applications, Biosens. Bioelectron. 15 (2000) 431–438.
[53] C. Padeste, B. Steiger, A. Grubelnik, L. Tiefenauer, Redox labelled avidin for enzyme sensor architectures, Biosens. Bioelectron. 19 (2003) 239–247.
[54] B. Steiger, C. Padeste, A. Grubelnik, L. Tiefenauer, Molecular assembly of redox-conductive ferrocene–streptavidin conjugates — towards bio-electrochemical devices, Electrochim. Acta 48 (2003) 761–769.
[55] C. Padeste, B. Steiger, A. Grubelnik, L. Tiefenauer, Molecular assembly of redox-conductive ferrocene–streptavidin conjugates — towards bio-electrochemical devices, Biosens. Bioelectron. 20 (2004) 545–552.
[56] S.J. Park, T.A. Taton, C.A. Mirkin, Array-based electrical detection of DNA with nanoparticle probes, Science 295 (2002) 1502–1506.
[57] K. Kerman, D. Ozkan, P. Kara, A. Erdem, B. Meric, P.E. Nielsen, M. Ozsoz, Label-free bioelectronic detection of point mutation by using peptide nucleic acid probes, Electroanalysis 15 (2003) 667–670.
[58] H. Xie, C.Y. Zhang, Z.Q. Gao, Amperometric detection of nucleic acid at femtomolar levels with a nucleic acid/electrochemical activator bilayer on gold electrode, Anal. Chem. 76 (2004) 1611–1617.
[59] F. Lucarelli, G. Marrazza, M. Mascini, Enzyme-based impedimetric detection of PCR products using oligonucleotide-modified screen-printed gold electrodes, Biosen. Bioelectron. 20 (2005) 2001–2009.
[60] A. Ferancova, M. Adamovski, P. Grundler, J. Zima, J. Barek, J. Mattusch, R. Wennrich, J. Labuda, DNA sensor for interaction of DNA with arsenic(III) and tin(II), Bioelectrochemistry 71 (2007) 33–37.
[61] D.W. Pang, H.D. Abruna, Micromethod for the investigation of the interactions between DNA and redox-active molecules, Anal. Chem. 70 (1998) 3162–3169.
[62] M. Mir, M. Alvarez, O. Azzaroni, L. Tiefenauer, W. Knoll, Molecular architectures for electrocatalytic amplification of oligonucleotide hybridization, Anal. Chem. 80 (2008) 6554–6559.
[63] M. Yang, H.C.M. Yau, H.L. Chan, Adsorption kinetics and ligand-binding properties of thiol-modified double-stranded DNA on a gold surface, Langmuir 14 (1998) 6121–6229.
[64] F. Mallard, G. Marchand, F. Giont, R. Campagnolo, Opto-electronic DNA chip: high performance chip reading with an all-electric interface, Biosens. Bioelectron. 20 (2005) 1813–1820.
[65] Z.-L. Zhi, Y. Morita, S. Yamamura, E. Tamiya, Microfabrication of encoded microparticle array for multiplexed DNA hybridization detection, Chem. Commun. 19 (2005) 2448–2450.
[66] X. Yao, X. Li, F. Toledo, C. Zurita-Lopez, M. Gutova, J. Momand, F.M. Zhou, Sub-attomole oligonucleotide and p53 cDNA determinations via a high-resolution surface plasmon resonance combined with oligonucleotide-capped gold nanoparticle signal amplification, Anal. Biochem. 354 (2006) 220–228.
[67] X. Su, Y.J. Wu, R. Robelek, W. Knoll, QCM DNA hybridization sensor with SPR detn, Langmuir 21 (2005) 348–353.
[68] Y. Okahata, Y. Matsunobu, K. Ijiro, M. Mukae, A. Murakami, K. Makino, Hybridization of nucleic acids immobilized on a quartz microbalance, J. Am. Chem. Soc. 114 (1992) 8299–8300.
[69] J. Fritz, M.K. Baller, H.P. Lang, H. Rothuizen, P. Vettiger, E. Meyer, H.J. Guntherodt, C. Gerber, J.K. Gimzewski, Translating biomolecular recognition into nanomechanics, Science 288 (2000) 316–318.
[70] K.M. Hansen, H.F. Ji, G.H. Wu, R. Datar, R. Cote, A. Majumdar, T. Thundat, Cantilever-based optical deflection assay for discrimination of DNA single-nucleotide mismatches, Anal. Chem. 73 (2001) 1567–1571.
[71] X. Su, D.N.A. Covalent, immobilization on polymer-shielded silver-coated quartz crystal microbalance using photobiotin-based UV irradiation, Biochem. Biophys. Res. Commun. 290 (2002) 962–966.
[72] J. Wang, M. Jiang, B. Mukherjee, On-demand electrochemical release of DNA from gold surfaces, Bioelectrochemistry 52 (2000) 111–114.
[73] I. Willner, F. Patolsky, Y. Weizmann, B. Willner, Amplified detection of single-base mismatches in DNA using microgravimetric quartz-crystal-microbalance transduction, Talanta 56 (2002) 847–856.
[74] X. Su, R. Robelek, Y. Wu, G. Wang, W. Knoll, Detection of point mutation and insertion mutations in DNA using a quartz crystal microbalance and MutS, a mismatch binding protein, Anal Chem. 76 (2004) 489–494.
[75] T. Hianik, V. Ostatna, M. Sonlajtnerova, I. Grman, Influence of ionic strength, pH and aptamer configuration for binding affinity to thrombin, Bioelectrochemistry 70 (2007) 127–133.
[76] J. Pribyl, M. Hepel, P. Skladal, Piezoelectric immunosensors for polychlorinated biphenyls operating in aqueous and organic phases, Sens. Actuators B 113 (2006) 900–910.
[77] M. Hepel, in: A. Wieckowski (Ed.), Interfacial Electrochemistry, M. Dekker, New York, 1999, pp. 599–631.
[78] F. Caruso, E. Rodda, D. Furiong, K. Niikura, Y. Okahata, Quartz crystal microbalance study of DNA immobilization and hybridization for nucleic acid sensor development, Anal. Chem. 69 (1997) 2043–2049.
[79] R.K. Saiki, D.H. Gelfand, S. Stoffel, S.J. Scharf, R.J. Higuchi, G.T. Horn, K.B. Mullis, H.A. Erlich, Primer-directed enzymatic amplification of DNA with a thermostable DNA polymerase, Science 239 (1988) 487–491.
[80] S. Bruckenstein, M. Shay, Experimental aspects of use of the quartz crystal microbalance in solution, Electrochim. Acta 30 (1985) 1295–1300.
[81] G. Sauerbrey, Verwendung von Schwingquarzcn zur Wagung d nner Schichten und zur Mikrowagung, Z. Phys. 155 (1959) 206–222.
[82] S. Trasatti, O.A. Petrii, Real surface area measurements in electrochemistry, Pure Appl. Chem. 63 (1991) 711.
[83] H.O. Finklea, S. Avery, M. Lynch, T. Furtsch, Blocking oriented monolayers of alkyl mercaptans on gold electrodes, Langmuir 3 (1987) 409–413.
[84] J. Spinke, M. Liley, H.J. Guder, L. Angermaier, W. Knoll, Molecular recognition at self-assembled monolayers: the construction of multicomponent multilayers, Langmuir 9 (1993) 1821–1825.
[85] D.Y. Cupo, K.E. Wetterhahn, Cancer Res. 145 (1985) 1146–1151.
[86] J.W. Hamilton, K.E. Wetterhahn, Carcinogenesis 7 (1986) 2085–2088.
[87] C.A. Miller, M. Costa, Mol. Carcinog. 1 (1988) 125–133.

[88] G. Pratviel, J. Bernadou, B. Meunier, Carbon–hydrogen bonds of DNA sugar units as targets for chemical nucleases and drugs, Angew. Chem., Int. Ed. 43 (1995) 746–769.
[89] C.J. Burrows, J.G. Muller, Chem. Rev. 98 (1998) 1109–1151.
[90] M. Purcell, J.F. Neault, H. Malonga, H. Arakawa, R. Carpentier, H.A. Tajmir-Riahi, Interactions of atrazine and 2, 4-D with human serum albumin studied by gel and capillary electrophoresis, and FTIR spectroscopy, Biochim. Biophys. Acta 1548 (2001) 129–138.
[91] J. SantaLucia, H.T. Allawi, P.A. Seneviratne, Improved nearest-neighbor parameters for predicting DNA duplex stability, Biochemistry 35 (1996) 3555–3562.
[92] M.C. Williams, I. Rousinal, Force spectroscopy of single DNA and RNA molecules, Curr. Opin. Struct. Biol. 12 (2002) 330–336.
[93] P. Yakovchuk, E. Protozanova, M.D. Frank-Kamenetskii, Base-stacking and base-pairing contributions into thermal stability of the DNA double helix, Nucleic Acids Res. 34 (2006) 564–574.
[94] J. SantaLucia, A unified view of polymer, dumbbell, and oligonucleotide DNA nearest-neighbor thermodynamics, Proc. Natl. Acad. Sci. USA 95 (1998) 1460–1465.
[95] N. Sugimoto, S. Nakamo, M. Yoneyama, K. Honda, Improved thermodynamic parameters and helix initiation factor to predict stability of DNA duplexes, Nucleic Acids Res. 24 (1996) 4501–4505.
[96] M.J. Doktycz, R.F. Goldstein, T.M. Paner, F.J. Gallo, A.S. Benight, Studies of DNA dumbbells I. Melting curves of 17 DNA dumbbells with different duplex stem sequences linked by T4 endloops: evaluation of the nearest-neighbor stacking interactions in DNA, Biopolymers 32 (1992) 849–864.
[97] R. Owczarzy, P.M. Vallone, R.F. Goldstein, A.S. Benight, Studies of DNA dumbbells VII: evaluation of the next-nearest-neighbor sequence-dependent interactionsin duplex DNA, Biopolymers 52 (1999) 29–56.
[98] M.D. Frank-Kamenetskii, How the double helix breathes, Nature 328 (1987) 17–18.
[99] M. Gueron, M. Kochoyan, J.L. Leroy, A single mode of DNA base-pair opening drives imino proton exchange, Nature 328 (1987) 89–92.
[100] E. Protozanova, P. Yakovchuk, M.D. Frank-Kamenetskii, Stacked–unstacked equilibria at the nick site of DNA, J. Mol. Biol. 342 (2004) 775–785.